Journal of Rock Mechanics and Geotechnical Engineering 16 (2024) 26–40

Contents lists available at ScienceDirect

Journal of Rock Mechanics and Geotechnical Engineering

journal homepage: www.jrmge.cn

Qian Lecture

Insights into carbon dioxide sequestration into coal seams through coupled gas flow-adsorption-deformation modelling

Hywel Thomas [a], Min Chen [a,b,*]

[a] Geoenvironmental Research Centre, Cardiff School of Engineering, Cardiff University, Queen's Buildings, The Parade, Newport Road, Cardiff, CF24 3AA, UK
[b] Key Laboratory of Marine Geology, Tongji University, Shanghai, 200092, China

ARTICLE INFO

Article history:
Received 31 July 2023
Received in revised form
11 November 2023
Accepted 20 November 2023
Available online 2 December 2023

Keywords:
CO_2 geological storage
Coal seam
Adsorption
Desorption hysteresis

ABSTRACT

Injecting carbon dioxide (CO_2) into coal seams may unlock substantial carbon sequestration potential. Since the coal acts like a carbon filter, it can preferentially absorb significant amounts of CO_2. To explore this further, desorption of the adsorbed gas due to pressure drop is investigated in this paper, to achieve an improved understanding of the long-term fate of injected CO_2 during post-injection period. This paper presents a dual porosity model coupling gas flow, adsorption and geomechanics for studying coupled processes and effectiveness of CO_2 sequestration in coals. A new adsorption–desorption model derived based on thermodynamics is incorporated, particularly, the desorption hysteresis is considered. The reliability of the proposed adsorption-desorption isotherm is examined via validation tests. It is indicated that occurrence of desorption hysteresis is attributed to the adsorption-induced pore deformation. After injection ceases, the injected gas continues to propagate further from the injection well, while the pressure in the vicinity of the injection well experiences a significant drop. Although the adsorbed gas near the well also decreases, this decrease is less compared to that in pressure because of desorption hysteresis. The unceasing spread of CO_2 and drops of pressure and adsorbed gas depend on the degree of desorption hysteresis and heterogeneity of coals, which should be considered when designing CO_2 sequestration into coal seams.

1. Introduction

It is well-known that global warming can affect changes in global climate pattern (Abbass et al., 2022; Masson-Delmotte et al., 2022). It is reported that the globally-averaged temperatures is 0.99 °C warmer than the middle twentieth century mean (NASA, 2017). This environmental concern is mainly due to the significant emission of greenhouse gases into atmosphere. The greenhouse gases include carbon dioxide (CO_2), methane (CH_4) and nitrogen oxide (NO), and some manufactured gases like chlorofluorocarbons (CFCs) (Al-Yasiri and Géczi, 2021). According to Mavor et al. (2002) and Ritchie et al. (2020), CO_2 emissions are the primary driver of global climate change. It is found that the CO_2 concentration in the atmosphere has rose significantly from 280 ppm in 1750 to 410 ppm in 2020 over last two centuries (Ali et al., 2022; Yoro and Daramola, 2020). Therefore, reduction of CO_2 emission into atmosphere is a major aspect of mitigation of global warming effects.

Many initiatives have been proposed to reduce CO_2 emissions, including utilisation of carbon-free renewable energy sources (e.g. wind, solar), CO_2 capture and storage (CCS) in geological formations (Wei et al., 2023). Among these means, CCS has been broadly recognised as a potential technique to mitigate anthropogenic CO_2 emissions. There are some primary CO_2 geological sequestration sinks including depleted oil and gas reservoirs, saline aquifers, basaltic rocks and coalbeds (Tomić et al., 2018). Among them, coal seams are significant because of their huge reserves and collocation with industrial scale CO_2 emission sources like power generation plants. Since the CO_2 adsorption capacity is higher than CH_4 in coals, existing coalbed methane (CBM) can be displaced using CO_2 and increase the gas recovery, known as enhanced coalbed methane (CO_2-ECBM) recovery (Asif et al., 2022; Godec et al., 2014; Kuang et al., 2023). On the one hand, the life of CBM fields can be

* Corresponding author. Geoenvironmental Research Centre, Cardiff School of Engineering, Cardiff University, Queen's Buildings, The Parade, Newport Road, Cardiff, CF24 3AA, UK.
E-mail address: 23518@tongji.edu.cn (M. Chen).

Peer review under responsibility of Institute of Rock and Soil Mechanics, Chinese Academy of Sciences.

https://doi.org/10.1016/j.jrmge.2023.11.004

extended, on the other hand, CBM production can also offset the cost of CO_2 storage. Many pilot trials of CO_2-ECBM have been completed or are currently underway or planned, such as San Juan Fairway ECBM project in USA (Reeves et al., 2003), RECOPOL pilot trial in Poland (van Bergen et al., 2006), Fenn Big Valley and Mannville pilot tests in Canada (Yang et al., 2023), Qinshui test in China (Wong et al., 2007) and Yubari test in Japan (Fujioka et al., 2010).

Naturally fractured coal is generally characterized by dual porosity model, i.e. almost uniformly spaced natural fractures (cleats) and porous coal matrices (see Fig. 1a) (Hosking et al., 2020). Generally, gas migration in coals occurs at three processes: injected CO_2 firstly leaks into cleat system from injection well. And then the CO_2 diffuses into coal matrices and adsorbs onto the pore surface (Chen et al., 2019). Fig. 1b represents the transport process of CO_2 in coals. The gas migration in cleat network is mainly controlled by coal permeability. Numerous experimental studies have been performed for exploring the change in coal permeability during gas transport (e.g. Pan et al., 2010; Wang et al., 2018a; Yao et al., 2023; Zhang et al., 2019). Similar to other fractured rocks, the coal permeability is stress dependent, showing an exponential relationship between the effective stress and permeability. In addition, the gas adsorption/desorption induced coal swelling/shrinkage can also lead to significant change in coal permeability (e.g. Meng and Li, 2017; Pan and Connell, 2012; Seidle and Huitt, 1995; Wierzbicki et al., 2014). Various permeability models have been developed to capture the changes in permeability, details were presented in (Pan and Connell, 2012). Although modelling permeability has incorporated the influences of both effective stress and swelling/shrinkage, the changes in either stresses or strains were

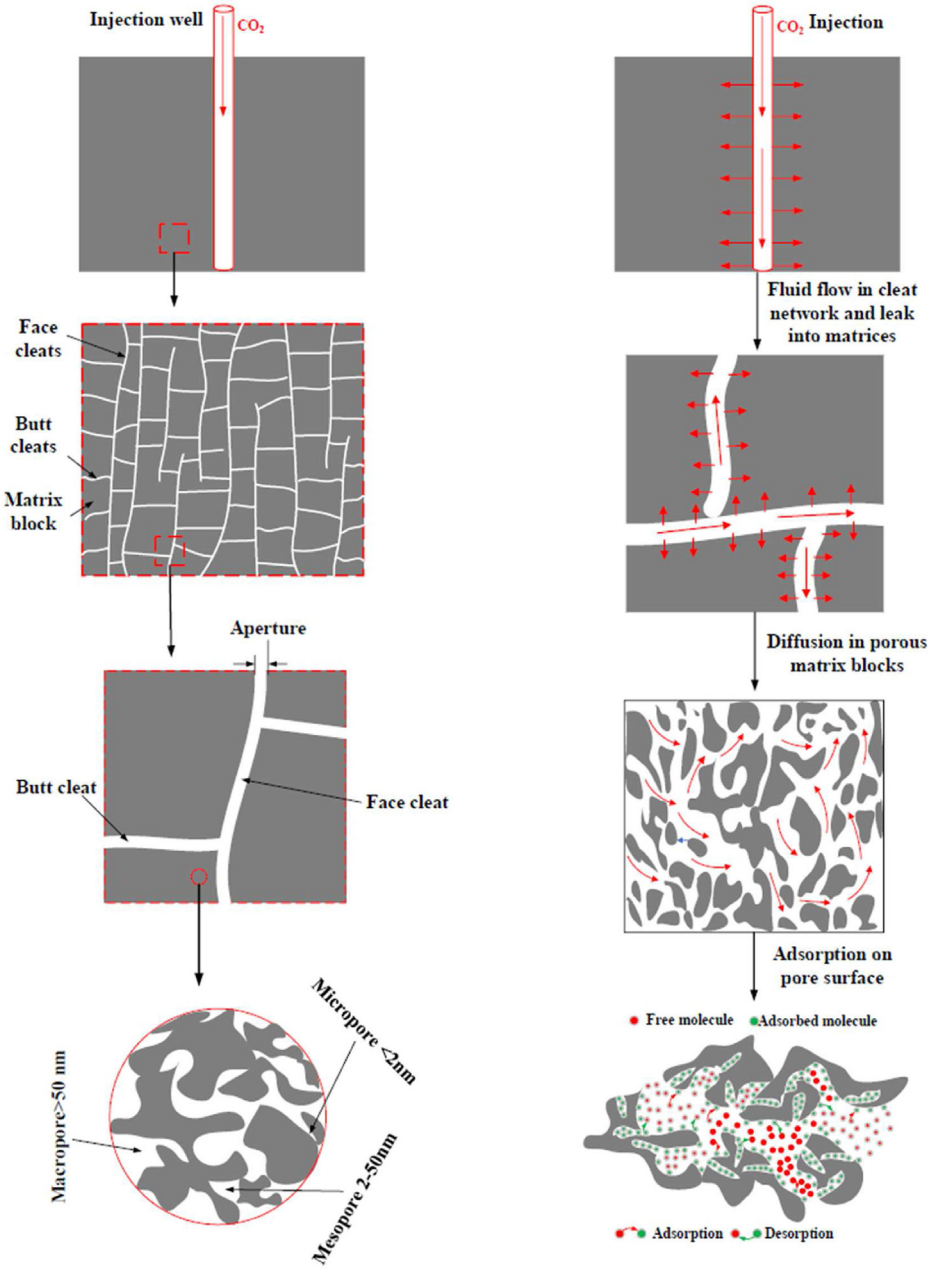

Fig. 1. (a) Schematic diagram of multi-scale pore structure of coals and (b) Gas transport process in coals.

superposed to calculate the total change in stresses or strains. These permeability models only hold based on an assumption that change in stress or strain due to fluid pressures is unrelated to that in coal swelling/shrinkage induced stress or strain. Most experimental tests on coal swelling/shrinkage were performed under non constrain conditions, leading to an overestimate compared to in situ stress conditions (Gu and Chalaturnyk, 2006). Besides, the in situ stresses or strains of coal seams are dynamic during gas injection, which is challenge to experimental measurements.

Adsorption onto the pore surface of coal matrices is considered to be the primary gas retention mechanism of coal seams, which is differ significantly from conventional gas reservoirs (Busch and Gensterblum, 2011). The gas adsorption behaviour in coals is impacted by some controllable factors including pressure, temperature, gas types, coal rank, moisture content (Chattaraj et al., 2016; Zhang et al., 2016). For example, because of smaller molecular size and coal pore structure, CO_2 shows a much higher adsorption affinity compared to CH_4 and N_2 (Strapoc, 2007). Gas adsorption is negatively affected by temperature and moisture content. Gas retention mechanism in coals is primarily a physical sorption due to weak van der Waals force of attraction; this implies that adsorbed gases can be released from coals when conditions for adsorption vary. However, many experimental studies shown that gas desorption is generally not a fully reversible, the adsorption isotherm is different from the desorption isotherm. This phenomenon is known as desorption hysteresis (e.g. Bell and Rakop, 1986; Wang et al., 2014; Zhou et al., 2020). However, most of current work focused on gas adsorption behaviour. For CO_2 storage in coal reservoirs, in addition to gas adsorption, gas desorption will also occur after injection event stops, since the pressure will decline with continuous propagation further (Chen et al., 2023; Wang et al., 2014). Understanding desorption hysteresis behaviour is of significance to evaluate storage efficiency of injected CO_2 in coal seams.

In addition to desorption hysteresis scenario, the coal reservoir heterogeneity is also an important factor influencing the long-term fate of sequestrated CO_2. Coal heterogeneity effect has been considered in many studies. For example, the work by Özgen Karacan and Okandan (1999) and Tan et al. (2018) demonstrated the effect of coal heterogeneity on CBM recovery, the homogenization assumption may cause large errors. In spite of the significance of heterogeneity effect, few attempts have made to explore the heterogeneity effects on CO_2 storage. This is another important issue this work attempts to address.

The objective of this work is to present an effective model for studying the gas flow and storage behaviour in heterogeneous coal seams based on our previous studies (Chen et al., 2022a, 2023). The uniqueness of this work includes:

(1) A coupled gas flow-adsorption/desorption-geomehcanics model for CO_2 sequestration is presented, in which the adsorption hysteresis is considered.
(2) The coupled processes and long-term storage effectiveness of CO_2 in coals with different degrees of hysteresis are analysed.
(3) Coal heterogeneity effect on long term effectiveness of CO_2 storage in coals is also considered in this work.

The following is outline of this work: the adsorption-desorption isotherm based on thermodynamics is derived in Section 2. In Section 3, the development of a numerical model coupling gas flow, adsorption and deformation behaviour is detailed. Validation tests for examining model reliability are shown in Section 4. Section 5 presents the mechanism for gas desorption hysteresis is revealed and the temporal-spatial evolutions of pressure and adsorbed CO_2 during injection and post-injection periods. Conclusions are summarized in Section 6.

2. Adsorption-desorption model development

Coal is considered to be composed of inter-linked polymer of a certain molecular weight, along with a structure formed by aggregations of aromatic macro-molecular chains (Ward and Suárez-Ruiz, 2008). The coal matrices have different size pores, which provide a much large internal surface for gas residence (see Fig. 1a). According to Chen et al. (2023), the pore surface of coals is energetically heterogeneous, different adsorption sites are contained. The patchwise model can be employed for representing the topography of adsorption sites whereby the heterogeneous surface is separated into different patches, each patch has the same interaction energy level (Ng et al., 2017), as shown in Fig. 2.

Therefore, each patch can be considered to be a homogeneous surface (Do, 1998; Ng et al., 2017), the revised Langmuir kinetics model can be used for describing adsorption kinetics (Do and Wang, 1998), expressed as

$$\frac{\mathrm{d}C_{si}(E_i)}{\mathrm{d}t} = k_{ai}\left(-\frac{E_{ai}}{RT}\right)p(C_{Li} - C_{si}) - k_{di}\left(-\frac{E_{di}}{RT}\right)C_{si} \tag{1}$$

where C_{si} is the adsorbed amount at each patch; C_{Li} is the local adsorption capacity at ith patch; k_{ai} and k_{di} are the rate constants; E_{ai} and E_{di} are the activation energies for adsorption and desorption, respectively; p is the pressure; T is the temperature; and R is the universal gas constant.

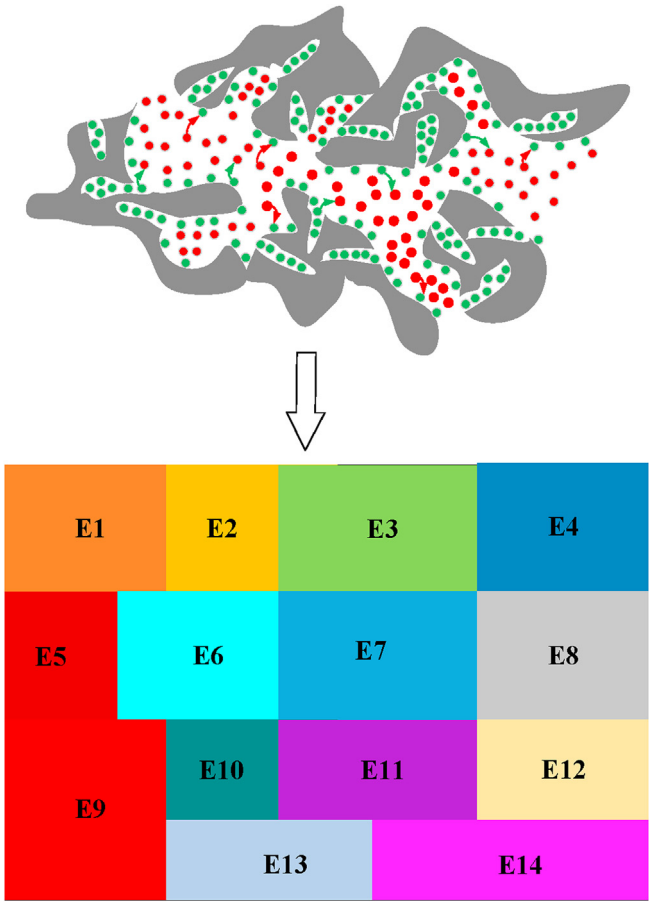

Fig. 2. Schematic illustration of energetically heterogeneous surface conceptualized as patchwise topography via grouping the sites of the same energy of interaction with the adsorbate together in the same patch.

When reaching equilibrium, $\frac{dC_{si}}{dt} = 0$, Eq. (1) is reduced to Langmuir isotherm equation (Do and Wang, 1998) as

$$\theta_i(E_i) = \frac{C_{si}}{C_{Li}} = \frac{K_i(E_i)p}{1 + K_i(E_i)p} \tag{2}$$

where $K_i(E_i) = \frac{k_{ai}}{k_{di}}$, $E_i = E_{di} - E_{ai}$ is the difference between adsorption and desorption energy for a given patch, and θ_i is the fraction of local adsorption uptake.

The total fractional surface coverage θ_t is expressed in the following form:

$$\theta_t = \frac{C_s}{C_L} = \sum_{i=1}^{n} \frac{C_{Li}}{C_L}\frac{C_{si}}{C_{Li}} = \sum_{i=1}^{n} F_i(E_i)\theta_i(E_i) \tag{3}$$

where C_s is the total amount adsorbed, which is calculated by summing adsorption uptake at all available patches, i.e. $C_s = \sum_{i=1}^{n} C_{si}$; C_L is the maximum adsorbed amount, $C_L = \sum_{i=1}^{n} C_{Li}$; and $F_i(E_i) = \frac{C_{Li}}{C_L}$, is the fraction of local adsorption sites to total sites.

Mathematically, the total fractional surface coverage θ_t can be expressed by the integration as

$$\theta_t = \int_0^{+\infty} \theta(E)F(E)dE \tag{4}$$

where E is the variable of integration.

By invoking the condensation approximation, θ in Eq. (4) reduces to a Heaviside step function (Panczyk and Rudzinski, 2002): $\theta(E) = 0$ when $E < E_c$; and $\theta(E) = 1$ when $E \geq E_c$, in which E_c is the critical energy level of the adsorbate molecule.

Therefore, Eq. (4) reduces to

$$\theta_t = \int_{E_c}^{+\infty} F(E)dE \tag{5}$$

In the case of patchwise topography, $F(E)$ in Eq. (5) represents adsorption energy distribution function. Quasi-Gaussian distribution has been successfully applied to characterize the energy distribution of adsorption sites (Ng et al., 2017; Panczyk and Rudzinski, 2002). In this study, it is also employed to capture the adsorption on energetically heterogeneous solid surfaces, written as

$$F(E) = \frac{1}{c}\frac{\exp\left(\frac{E-E_0}{c}\right)}{\left[1 + \exp\left(\frac{E-E_0}{c}\right)\right]^2} \tag{6}$$

where E_0 is the mathematical expectation, and c is the standard deviation.

Inserting Eq. (6) into Eq. (5) and integrating over available adsorption sites produce

$$\theta_t = \frac{1}{1 + \exp\left(\frac{E_c-E_0}{c}\right)} \tag{7}$$

Application of $E_c = -RT\ln(Kp)$ allows equation above to become (Dobruskin, 1998):

$$\theta_t = \frac{\left[Kp\exp\left(\frac{E_0}{RT}\right)\right]^{\frac{RT}{c}}}{1 + \left[Kp\exp\left(\frac{E_0}{RT}\right)\right]^{\frac{RT}{c}}} \tag{8}$$

Under isothermal condition, if define $K\exp\left(\frac{E_0}{RT}\right) = K_{LF}$ and $\frac{RT}{c} = n$, Eq. (8) can be expressed in the form of Langmuir-Freundlich isotherm:

$$\theta_t = \frac{(pK_{LF})^n}{1 + (pK_{LF})^n} \tag{9a}$$

$$C_s = C_L\theta_t = \frac{C_L(pK_{LF})^n}{1 + (pK_{LF})^n} \tag{9b}$$

It is can be seen From Eq. (9) that Langmuir isotherm is a particular form of Langmuir-Freundlich isotherm, it is obtained by defining $n = 1$.

For gas desorption, due to hysteresis scenario, the desorption isotherm generally deviates from adsorption isotherm. Also, when developing desorption isotherm, the following boundary conditions should be considered (see Fig. 3):

(1) At state M, depressurization begins, desorption isotherm is intersected with adsorption isotherm, and the adsorption amounts at both isotherms are identical;
(2) There is no adsorbed gas when pressure drops to zero;
(3) If adsorption is completely irreversible, the adsorption amount is constant although pressure decreases;
(4) The desorption isotherm should coincide with sorption isotherm if the adsorption is fully reversible; and
(5) Desorption curve is dependent on the initial state where depressurization begins.

Considering three different adsorption energy states p_A, p_D and p_M, as shown in Fig. 3, the adsorption sites energy differences from state p_A to state p_D and from state p_M to state p_D are

$$\Delta E_{cAD} = E_{cA} - E_{cD} \tag{10a}$$

$$\Delta E_{cMD} = E_{cA} - E_{cD} \tag{10b}$$

The ratio of ΔE_{cAD} to ΔE_{cMD} defines an index (HI):

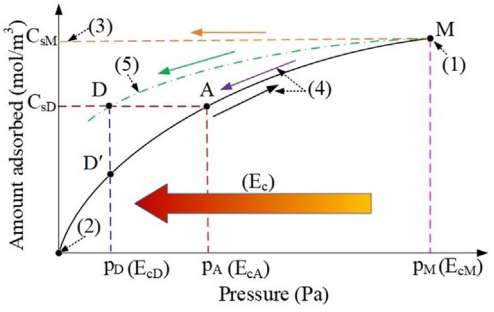

Fig. 3. Schematic representation of states M, A and D for desorption isotherm development: State M is the adsorption state where desorption initiates, state D is the experimentally measured desorption state, and state A and state D' corresponds to the hypothetical fully reversible desorption state. Black, yellow, purple and green arrows indicate adsorption isotherm, desorption isotherm for irreversible adsorption, fully reversible desorption and experimental desorption isotherm.

$$HI = \frac{\Delta E_{cAD}}{\Delta E_{cMD}} = \frac{\ln p_D - \ln p_A}{\ln p_D - \ln p_M} \tag{11}$$

HI can be used to quantify the degree of hysteresis. Sander et al. (2005) defines a similar thermodynamic index of irreversibility (*TII*) to evaluate the degree of hysteresis.

After rearrangement, Eq. (11) becomes

$$p_A = {p_D}^{1-HI} {p_M}^{HI} \tag{12}$$

Substituting Eq. (12) into Eq. (9) and replacing p_D with p allow desorption isotherm to be expressed as

$$C_s = \frac{C_L \left(K_{LF} {p_M}^{HI} p^{1-HI}\right)^n}{1 + \left(K_{LF} {p_M}^{HI} p^{1-HI}\right)^n} \tag{13}$$

Eq. (13) still takes the form Langmuir-Freundlich isotherm, it satisfies the conditions mentioned above. For example, the parameter P_M reveals that the desorption curve depends on the initial pressure. Completely reversible adsorption process can be achieved via defining *HI* to be 0.

3. Modelling CO_2 sequestration in coals

As mentioned above, naturally fractured coal is usually characterized as dual porosity system, gas migration processes include fracture network flow, diffusion in coal matrices and adsorption onto pore surface of coal matrices. This section will present a coupled flow-adsorption-geomechanics model to represent gas migration processes in coals. In the following sections, the governing equations are presented.

3.1. Gas transport

The mass balance equation of gas flow is expressed as (Chen et al., 2019; Cui et al., 2022):

$$\frac{\partial}{\partial t}(c_\alpha \varphi_\alpha) + \nabla \cdot \boldsymbol{q}_\alpha = R_\alpha + \Gamma_\alpha \ (\alpha = \mathrm{m}, \mathrm{f}) \tag{14}$$

where c_α is gas concentration; φ_α is porosity; $\boldsymbol{q}_\alpha$ is flow fluxes; R_α is the sink/source term; Γ_α is the mass exchange rate between fracture continuum and matrix continuum; ∇ is the gradient operator; and m, f denote fracture continuum and matrix continuum, respectively.

The flux terms are expressed as

$$\boldsymbol{q}_\alpha = c_\alpha \boldsymbol{v}_\alpha \tag{15}$$

where $\boldsymbol{v}_\alpha$ is the flow velocity, it is expressed using Darcy's law as

$$\boldsymbol{v}_\alpha = -\frac{K_\alpha}{\mu} \nabla p_\alpha \tag{16}$$

where K_α is the coal permeability, μ is the gas viscosity, and p_α is the gas pressure. The permeability model development is detailed in Appendix A.

Considering the real gas law, the gas pressure can be given as

$$p_\alpha = Z_\alpha R T c_\alpha \tag{17}$$

where Z_α is the gas compressibility factor. Peng-Robinson equations of state or PR-EoS is used for calculation of gas compressibility factor in this work (Peng and Robinson, 1976).

Since gas adsorption only occurs in coal matrices, which acts as the sink/source for matrix continuum, expressed as

$$R_m = \rho_s \frac{dC_s}{dt} \tag{18}$$

where ρ_s is the density of coal.

It is assumed that the gas transfer between the matrix and fracture is driven by the difference of concentration, written as (Chen et al., 2019)

$$\Gamma_\alpha = \frac{1}{\tau}\left(c_m - c_f\right) \tag{19}$$

where τ is the diffusion time (Liu et al., 2015).

3.2. Coal deformation

Considering dual poroelastic theory, the effective stress is expressed as (Chen et al., 2019; Pao and Lewis, 2002):

$$d\boldsymbol{\sigma}' = d\boldsymbol{\sigma} - \beta_m \boldsymbol{I} dp_m - \beta_f \boldsymbol{I} dp_f \tag{20}$$

where $\boldsymbol{\sigma}$ is the total stress tensor, $\boldsymbol{\sigma}'$ is the effective stress tensor, $\boldsymbol{I}$ is a vector with $\boldsymbol{I}^T = (1,1,1,0,0,0)$ and $(1,1,0)$ in three- and two-dimensions problems. $\beta_m = K/K_m - K/K_s$ and $\beta_f = 1 - K/K_m$ are the Biot's coefficients of the matrix and fracture, respectively; $K = E_Y/3(1-2\nu)$, is the bulk modulus, in which E_Y is the Young's modulus and ν is Poisson's ratio; and $K_m = E_{Ym}/3(1-2\nu)$, is the modulus of coal matrix with E_{Ym} being Young's modulus of the coal matrix and K_s is the modulus of solid constituent.

The stress-strain constitutive relation is defined as

$$d\boldsymbol{\sigma}' = \boldsymbol{D} d\boldsymbol{\varepsilon}^e \tag{21}$$

where $\boldsymbol{D}$ is the elastic stiffness tensor, and $\boldsymbol{\varepsilon}^e$ is the elastic strain vector.

The total strain can be expressed as

$$d\boldsymbol{\varepsilon} = d\boldsymbol{\varepsilon}^e + \frac{1}{3}\boldsymbol{I} d\varepsilon^s \tag{22}$$

where $\boldsymbol{\varepsilon}$ is the total strain vector, and ε^s is the sorption-induced volumetric strain.

The strain-displacement relation is written as

$$d\boldsymbol{\varepsilon} = \boldsymbol{B} d\boldsymbol{u} \tag{23}$$

where $\boldsymbol{u}$ is the displacement vector, and $\boldsymbol{B}$ is the strain-displacement matrix.

The swelling strain is considered to be linearly related with total adsorbed amount (e.g. Cui et al., 2007):

$$d\varepsilon^s = \varepsilon_L dC_s \tag{24}$$

where ε_L is the volumetric strain coefficient of coals.

3.3. Numerical approach

In this study, the aforementioned theoretical formulation is implemented into the in-house computer code, which has been gradually developed (e.g. Thomas and He (1997); Hosking et al. (2017); Chen et al. (2022b). In this computer code, the Galerkin weighted residual method is employed to spatially discretize the governing equations and an implicit mid-interval backward-difference time-stepping algorithm is used for temporal

discretization. Details can be found in Chen et al. (2022b). All the simulations in following section are completed using this in-house code.

4. Model validation against experimental data

This section presents a model validation exercise for examining the its reliability to predict gas adsorption behaviour in coals. The experimental data collected from published work (Dutta et al., 2011; Weishauptová et al., 2004) is used as benchmarks. More validation tests have been included in our previous work, for example, on unsaturated flow, coal permeability evolution, coal deformation and hydraulic-mechanical coupling (Chen et al., 2022a, 2022b). Weishauptová et al. (2004) measured the equilibrium adsorption behaviour of CH_4 in bituminous coal samples (coal A and coal B) and brown coal (coal C) using the gravimetric method. Coal A and coal B were from Upper Silesian coal basin and coal C from North Bohemian basin, respectively. All measurements were carried out at temperature of 298 K. Dutta et al. (2011) conducted experimental measurements of CH_4 and CO_2 adsorption on bituminous coal samples using manometric method, and the sorption isotherms of CH_4 and CO_2 were obtained. Here, the experimental results of on Bogra and Kenda coal samples in Dutta et al. (2011) were collected as benchmarks for validation exercises.

Table 1 presents the model parameters for validation against benchmarks from Weishauptová et al. (2004) and Dutta et al. (2011), which were obtained by matching the experimental data. Values of model parameters n and HI ranges from 0.793 to 0.983 and from 0.2 to 0.8, respectively, which fall within the range from 0 to 1. The comparisons between model predictions and the data published by Weishauptová et al. (2004) and Dutta et al. (2011) for pure CO_2 and CH_4 are ploted in Figs. 4 and 5, from which the good agreements can be observed, demonstrating the reliability of the model.

5. Numerical simulations of CO_2 sequestration in coal seams

5.1. Simulation setup

Depleted coal reservoirs have been recognised as a target formation for geological CO_2 storage (Reisabadi et al., 2022). This subsection designs a set of numerical simulations to unlock the mechanisms for CO_2 storage in depleted reservoirs. The two-dimensional (2D) region of 400 m × 400 m with a depth of 400 m is considered with a CO_2 injection at the centre. Considering the symmetry, only a quarter of domain is considered in the simulation (Fig. 6). It is assumed there is no CO_2 in coal initially. The initial vertical and horizontal stresses are 9 MPa and 6.3 MPa, respectively. Constant volume condition is used as boundary condition for coal deformation. A zero-flux boundary is used for gas flow. CO_2 is continuously injected at 6 MPa and injection ceases after 1 year. The simulation runs for 20 years. This simulation time is selected based on 5-year post-injection monitoring of stored CO_2 carried out by Mito and Xue (2011), which showed that the formation pressure became gradually stable from 1 years after injection stop. To ensure the long-term fate of injected CO_2, the simulation time is extended in this work. Four analysis points are set to show the coupled process of CO_2 in coal seams: P1 (10, 10), P2 (30, 30), P3 (50, 50), P4 (100, 100). Table 2 lists the material properties for numerical simulations, which are chosen from Chen et al. (2023).

Table 1
Parameters for validation against experimental data (Weishauptová et al., 2004; Dutta et al., 2011).

Sample	Gas type	Adsorption capacity, C_L (mg/g)	Constant, K_{LF} (MPa^{-1})	Exponent, n	Index, HI or TII
Coal-A	CH_4	11.31	2.12	0.956	0.63
Coal-B	CH_4	28.69	2.43	0.974	0.80
Coal-C	CH_4	29.46	4.67	0.925	0.79
Bogra	CH_4	24.5	0.33	0.983	0.28
Bogra	CO_2	182.78	0.22	0.820	0.39
Kenda	CH_4	18.94	0.27	0.902	0.20
Kenda	CO_2	178.04	0.22	0.793	0.42

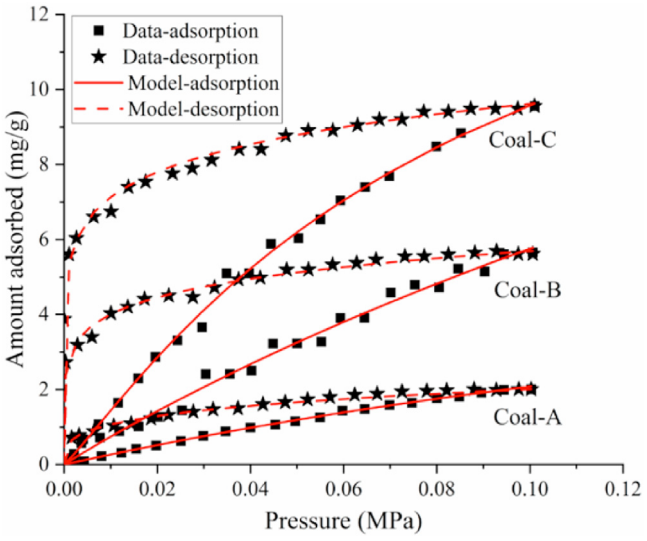

Fig. 4. Comparison between model predictions and experimental data on CH_4 adsorption/desorption on coal samples by Weishauptová et al. (2004).

5.2. Results and discussions

5.2.1. Mechanism for desorption hysteresis

Fig. 7 shows that site energy distributions under given conditions, which are calculated using Eqs. (6) and (13). It can be observed that mean site energy, E_0, can be increased due to gas-coal interaction. Compared to site energy distribution for adsorption isotherm, the sites with medial and higher binding energy experience an increasing trend after coal-gas interaction, while low energy sites show a significant drop. Burhan et al. (2019) and Li et al. (2019) have reported that adsorption energy is negatively correlated with pore size, this implies that the size of some pores becomes small due to gas-coal interaction. This change in pore structure revealed here is similar to laboratory observations by e.g. Wang et al. (2018b), Cheng et al. (2021) and Geng et al. (2022). It is believed that the alteration of pore structure can be ascribed to pore deformation and structural rearrangement as a result of gas adsorption (Larsen, 2004). An increase in smaller size pores leads to an increase in adsorption sites with higher binding energy. Consequently, desorption requires more activation energy, which is generated by a larger gas pressure drop, this is why the desorption hysteresis occurs.

5.2.2. Evolutions of pressure, adsorbed CO_2 and permeability

Figs. 8 and 9 show spatial distributions of gas pressure and adsorbed gas concentration at different times. The injected CO_2 moves outward in a radial pattern from the injection well and disperses within the coal seam, the pressure and adsorbed gas concentration distribute uniformly around the wellbore. After injection ceases (1 year), the injected gas propagates continuously,

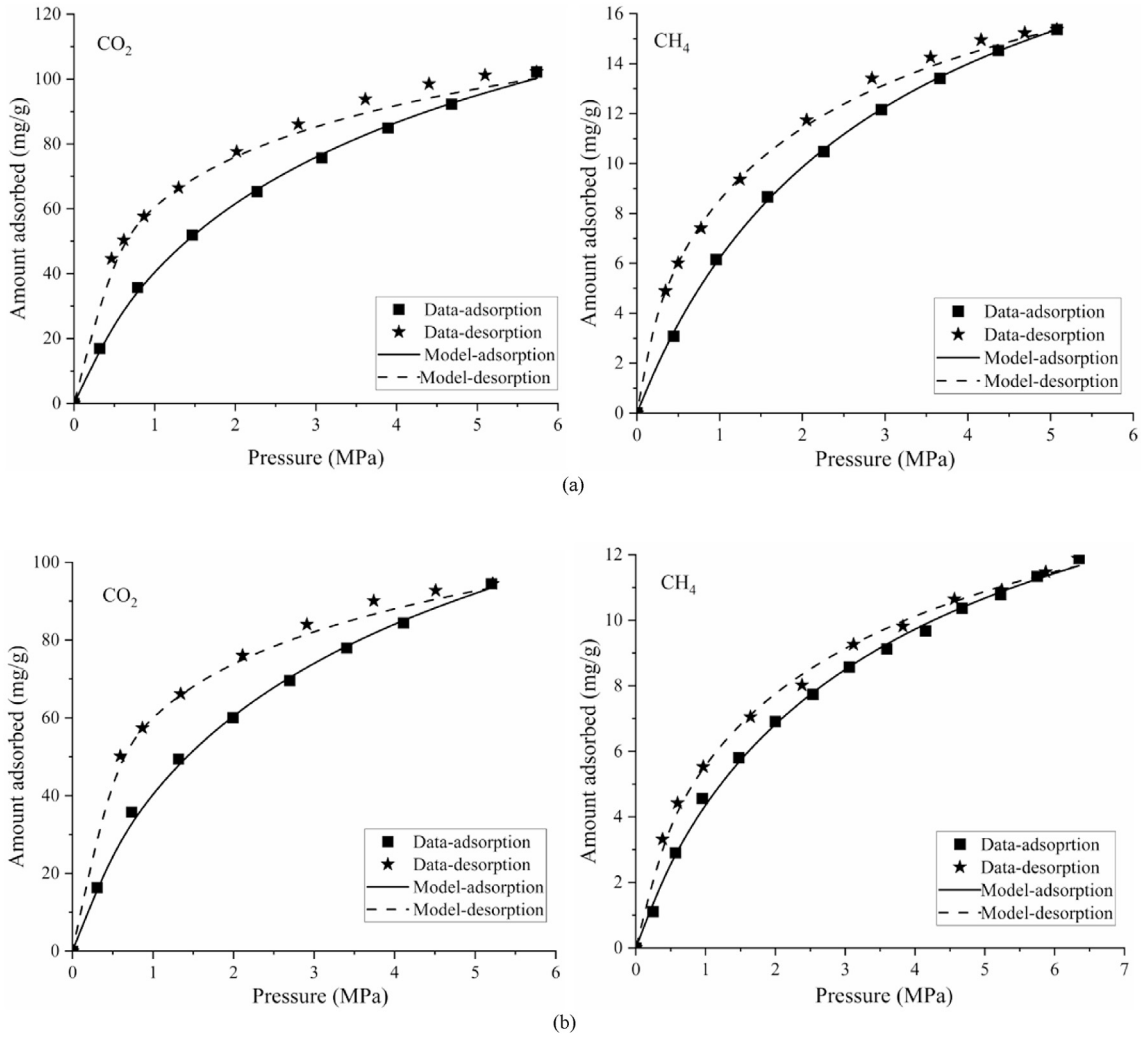

Fig. 5. Comparison of between model predictions and experimental data on (a) Bogra coal samples and (b) Kenda coal samples.

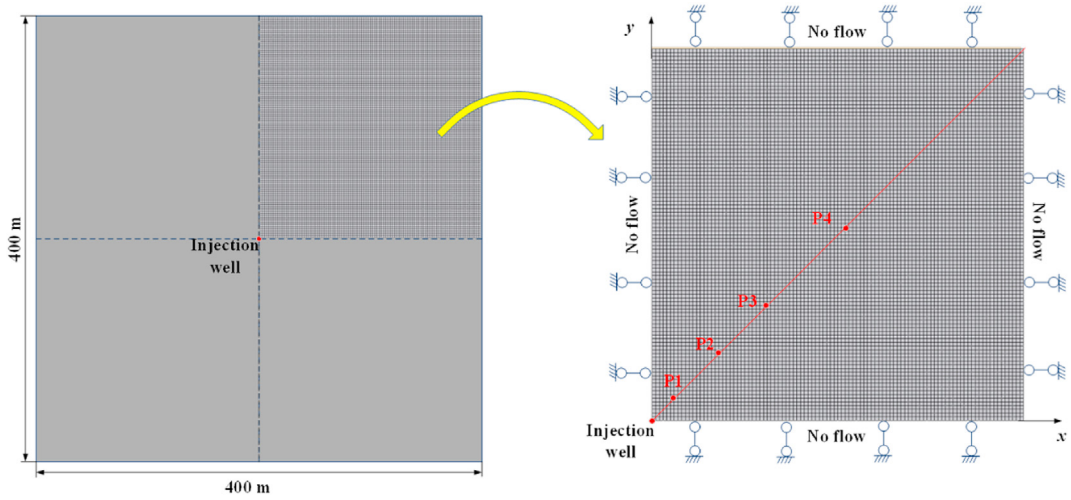

Fig. 6. Schematic diagram of model domain and boundary conditions.

leading to drop in pressure in the vicinity of injection well. Because of pressure drop, adsorbed gas will desorb and adsorbed gas concentration also undergoes a decrease. In particular, the drop in pressure and adsorbed CO_2 is most significant in the first year after injection stops, as shown in Fig. 10. The pressure near injection well decreases from 6 MPa to 1 MPa, in contrast, the decrease in

Table 2
Parameters for the numerical simulation.

Parameters	Units	Values
Porosity of coal matrix, φ_m		0.045
Porosity of fracture, φ_f		0.018
Initial permeability, K_{f0}	m^2	1×10^{-15}
Gas viscosity, μ	Pa s	1.84×10^{-5}
Density of coal, ρ_s	kg/m^3	1470
Elastic modulus of bulk coal, E_Y	GPa	1.86
Elastic modulus of coal matrix, E_{Ym}	GPa	9.3
Poisson's ratio, ν		0.32
Initial fracture compressibility, C_{f0}	MPa^{-1}	0.116
Fracture compressibility change rate, α_c	MPa^{-1}	0.25
Diffusion time, τ	s	2×10^5
Maximum adsorption amount, C_L	mol/kg	1.55
Constant of LF isotherm, K_{LF}	MPa^{-1}	0.496
Exponent of adsorption isotherm, n		0.86
Desorption hysteresis index, HI		0.3
Temperature, T	K	303

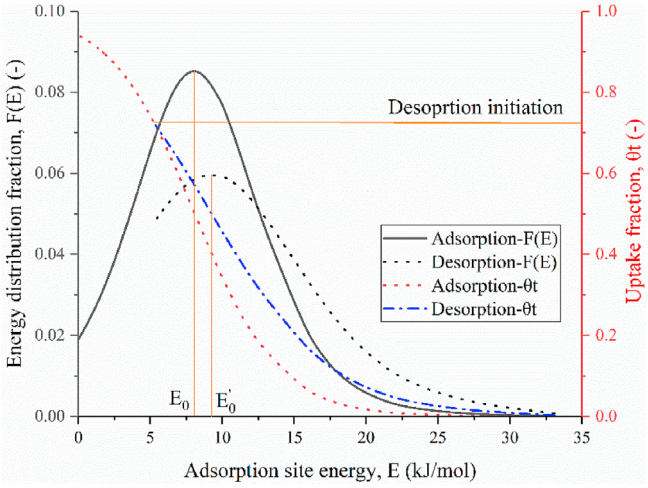

Fig. 7. Site energy distribution function $F(E)$ and cumulative uptake θ_t (given that $p_M = 6$ MPa).

adsorbed CO_2 concentration is less significant due to desorption hysteresis, which decreases from about 68 kg/m^3 to 46 kg/m^3. As time increases, the decreases of pressure and adsorbed CO_2 concentration slow down. For example, the pressures near well are 0.55 MPa, 0.38 MPa and 0.27 MPa after 5 years, 10 years and 20 years, respectively. The adsorbed gas concentration drops to 37 kg/m^3, 32 kg/m^3 and 28 kg/m^3, as shown in Fig. 10a.

After injection stop, pressure and adsorbed CO_2 concentration within the region far from injection well can still experience a little increase due to continuous gas spread, as shown in Fig. 10b and c. The gas pressure front arrives at approximately 93 m away from wellbore, after 20 years, it reaches about 197 m from wellbore, as shown in Fig. 10b. Nevertheless, the gas spread slows down as time goes. For example, the gas pressure front arrives at 148 m, 170 m, and 180 m after 5 years, 10 years and 10 years, respectively. This is because: (1) as the distance from the injection well grows, the area over which the gas spreads also expands; and (2) the pressure is almost identical in the area where CO_2 reaches, which leads to drop in the gas pressure gradient as time goes.

Fig. 10d shows permeability distribution along the diagonal at different times. It can be observed that variation of coal permeability is contrary to that of adsorbed CO_2. This is because CO_2 adsorption-induced swelling causes an increase in stresses within coal seam. The more CO_2 is adsorbed, the larger increase in stress is. The permeability is stress dependent, thus, it experiences a larger drop in the area near injection well. After injection stop, the desorption of CO_2 occurs as injected CO_2 continues to propagate further, which can lead to shrinkage of coal seams and reduction of stress of coal seams, therefore, the coal permeability can rebound in the area closed to injection well during post injection period, as shown in Fig. 10d.

Fig. 11 presents the temporal evolutions of pressure and adsorbed CO_2 concentration of monitoring points P1–P4. It is shown that the gas pressure and adsorbed CO_2 concentration within a 50-m range from the injection well begin to decrease immediately once injection ceases. The closer the monitoring point is to injection well, more rapidly the pressure and adsorbed CO_2 concentration drop. After 20 years, the gas pressure is almost the same in the region closed to wellbore. However, the difference of adsorbed gas concentrations between monitoring points is obvious since the desorption characteristics of gas in coals depends on the pressure at which pressure drop initiates (see Fig. 12). When the initialized pressure is larger, the drop in adsorbed gas concentration is rapider once injection ceases. From Fig. 12, we can observe that when the initialized pressure for desorption are different, the amounts of residual gas in coal are different although the gas pressure drops to the same value. Chen et al. (2023b) believed that a higher initial pressure marks the start of desorption, leading a greater portion of intermediate binding energy sites to transition into high binding energy sites. Consequently, under higher pressure condition, despite a more considerable pressure decrease, fewer adsorbed gas molecules are released when the starting pressure for desorption is higher, as shown in Fig. 12.

5.2.3. Influence of desorption hysteresis

Due to the significance of adsorption hysteresis, the effect of degree of hysteresis is analysed in this study, which is achieved through defining another two different hysteresis indices $HI = 0.6$, 0.9. Figs. 13 and 14 present the comparisons of pressure and adsorbed gas concentration evolutions for different degrees of hysteresis at monitoring points P1–P4. For stronger degree of desorption hysteresis, the pressure drop after injection stops is more significantly and rapidly, however, the adsorbed gas concentration shows an opposite changing pattern. There is a significant drop in adsorbed gas concentration when degree of hysteresis is less. The reason behind this scenario is that when the degree of desorption hysteresis intensifies, the number of available adsorption sites containing higher binding energy increases. Consequently, a larger pressure decrease is required for desorption of adsorbed CO_2, rendering it difficult for adsorbed CO_2 to desorb and return to the free phase. Meanwhile, the free phase CO_2 can continue to propagate further, leading to a drop in the concentration of free phase CO_2 in the region. As a result, the gas pressure in the region decreases more significantly, while the concentration of adsorbed CO_2 remains relatively higher. It can be inferred that because of substantial drop in pressure, the spread of CO_2 will become slower, and it might even cease when significant desorption hysteresis of CO_2 is present. This suggests that coal seams exhibiting strong desorption hysteresis are advantageous for the long-term sequestration of CO_2.

5.2.4. Influence of reservoir heterogeneity

The coal reservoir is highly heterogeneous, therefore, one objective of present work is to show the heterogeneity effects on CO_2 storage in coal seams. Here, the non-uniform permeability distribution is considered to show the impact of coal heterogeneity in flow conductivity. Fig. 15 shows the logarithmic distribution is used for generation of random permeability field used in simulation with a mean value of 1×10^{-15} m^2 and variance of 4×10^{-30},

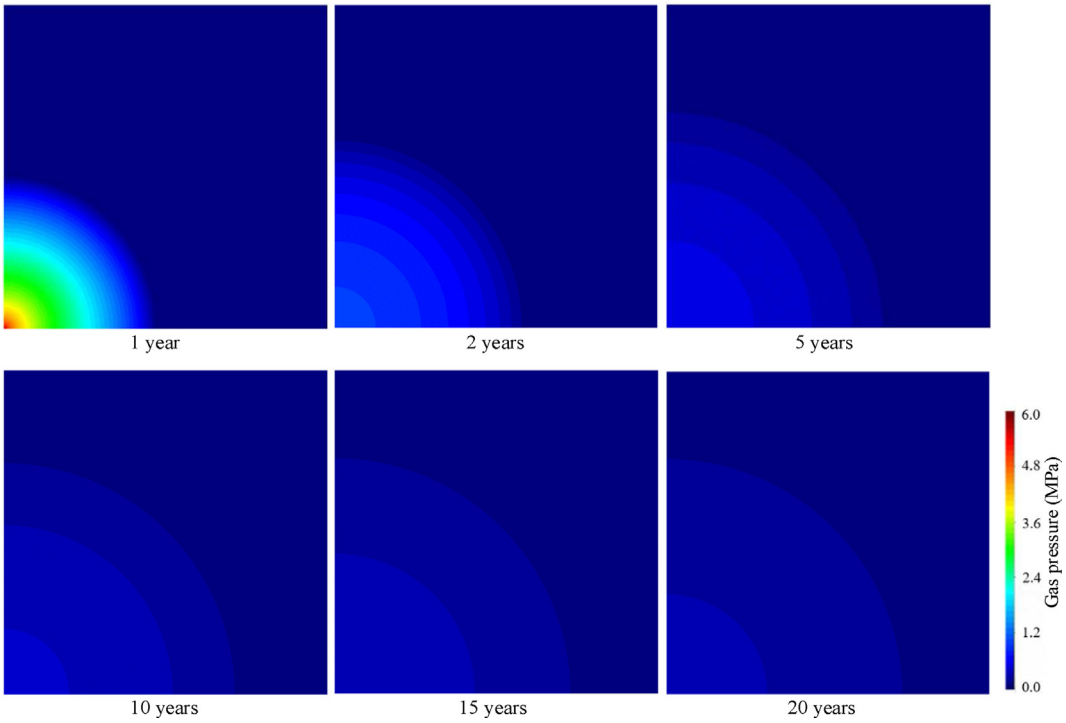

Fig. 8. Pressure distribution in the coal seam after 1 year, 2 years, 5 years, 10 years, 15 years and 20 years.

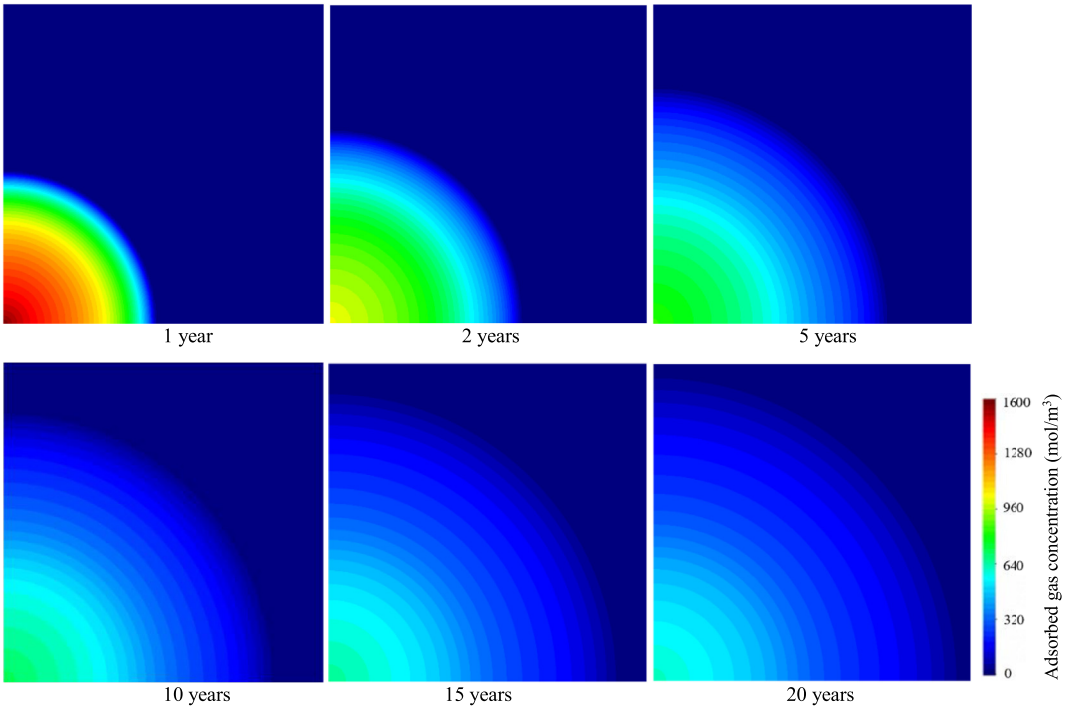

Fig. 9. Adsorbed gas concentration distribution in the coal seam after 1 year, 2 years, 5 years, 10 years, 15 years and 20 years.

other material properties are still assumed to be the same in the simulation domain. Figs. 16 and 17 present pressure and adsorbed CO_2 concentration distributions during injection and post-injection periods of operations. Compared to the homogeneous case (see Figs. 8 and 9), distributions of pressure and adsorbed CO_2 are non-uniform. The injected gas firstly flows into zone where the permeability is higher, leading to higher adsorbed gas concentration.

Particularly, the spread of injected CO_2 in coal seams when considering heterogeneity effect is slower than that under assumption of reservoir homogeneity. Fig. 18 shows the pressure and adsorbed CO_2 distribution along the diagonal. It can be seen

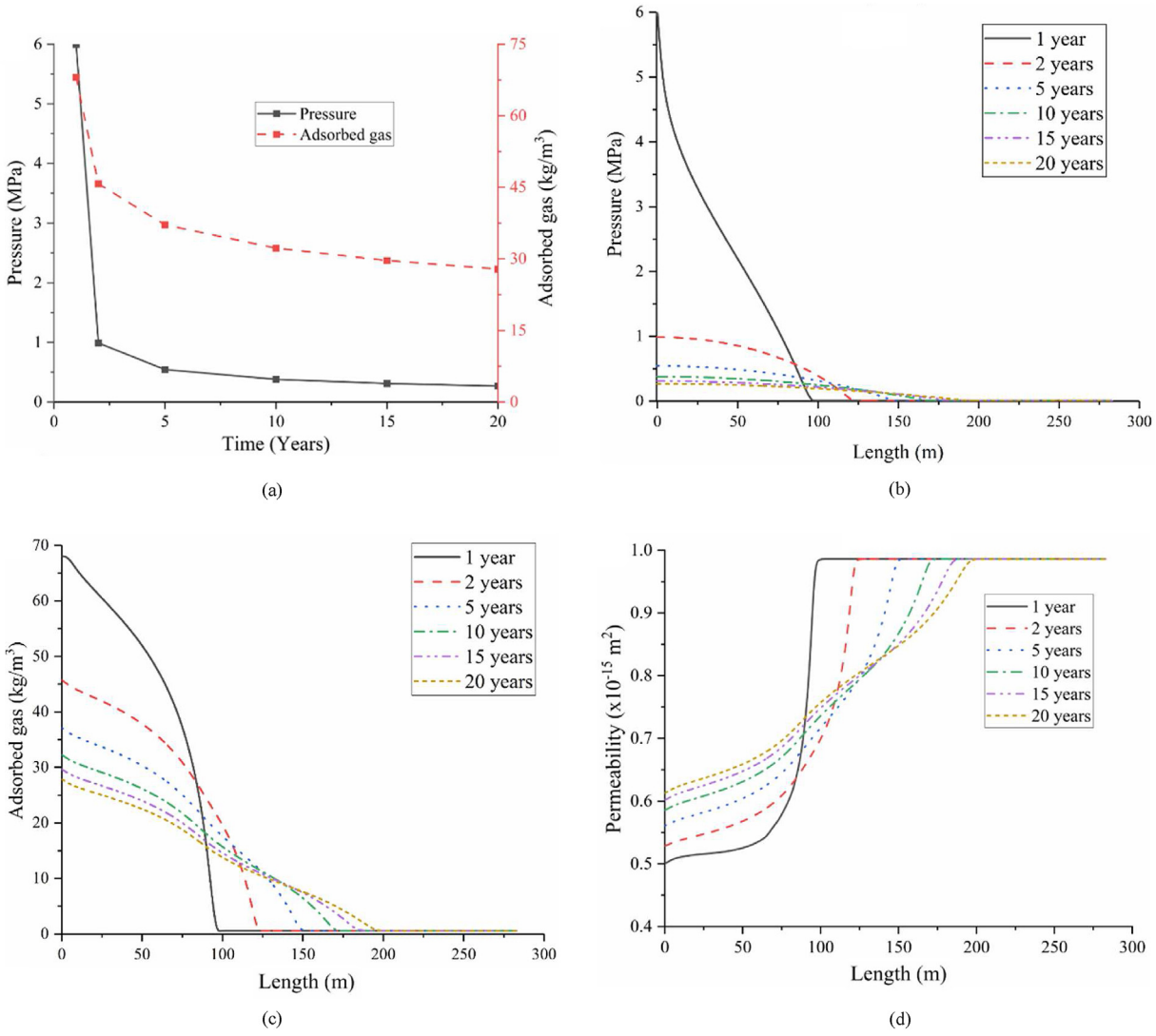

Fig. 10. (a) Evolution of pressure and adsorbed gas concentration near injection well, (b) pressure distribution, (c) adsorbed gas concentration distribution and (d) permeability distribution along the diagonal after 1 year, 2 years, 5 years, 10 years, 15 years and 20 years.

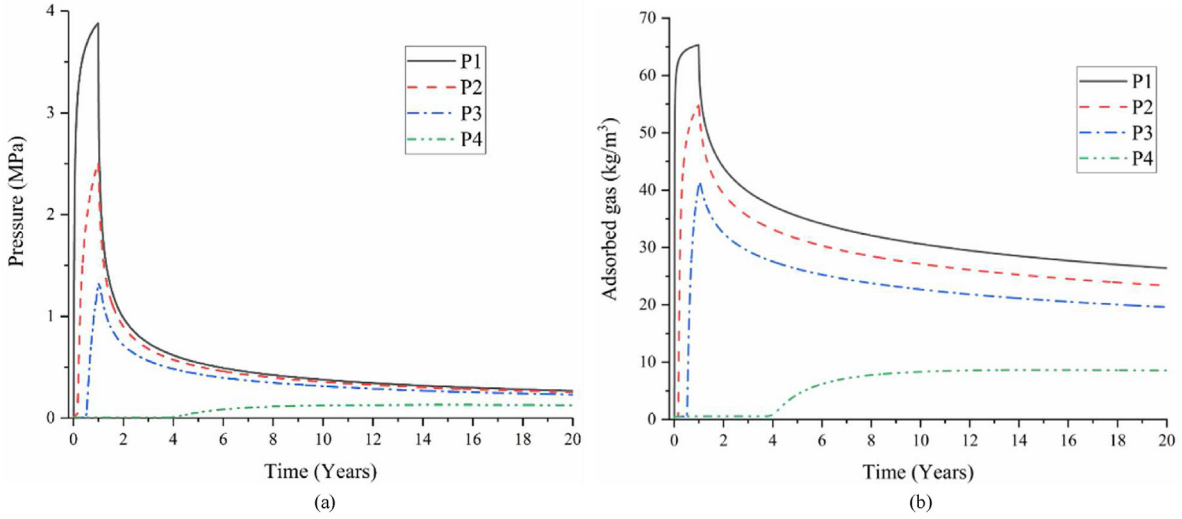

Fig. 11. Pressure and adsorbed gas concentration evolution at monitoring points P1–P4: (a) Pressure and (b) adsorbed gas concentration.

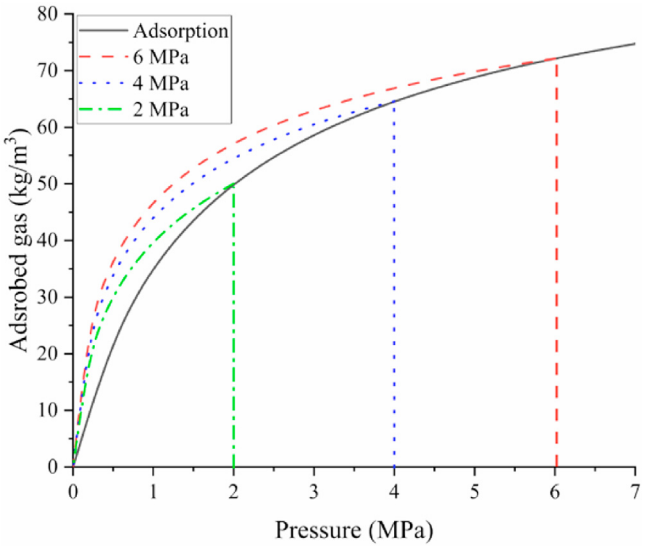

Fig. 12. Desorption isotherms for different initialized pressures.

that the gas front only reaches at distance of about 76 m and 155 m from injection well after 1 year and 20 years, respectively, which is smaller than that (93 m and 197 m) for homogeneous case (see Fig. 10). This implies that the heterogeneity effect on gas transport within coal seams is significant. It is worth pointing out that the random permeability field may be simplified, although the heterogeneity effects can be observed from the simulation results, more attempts to reservoir heterogeneity effect using advanced geostochastic methods like Kriging distribution should be made in future research work for engineering applications.

5.2.5. *Implications for CO_2 storage in coal seams*

Understanding the coupled processes is important for geological CO_2 sequestration. To this end, this study presents a coupled flow-adsorption-geomechanics model, particularly, the desorption hysteresis is considered. It offers an effective approach to estimate the CO_2 leakage during injection period and continuous migration after injection cease. These results can provide certain guidance for design and management of CO_2 injection into coal seams. For example, it facilitates pressure selection for CO_2 injection when the amount of injected CO_2 is identified. The distance between injec-

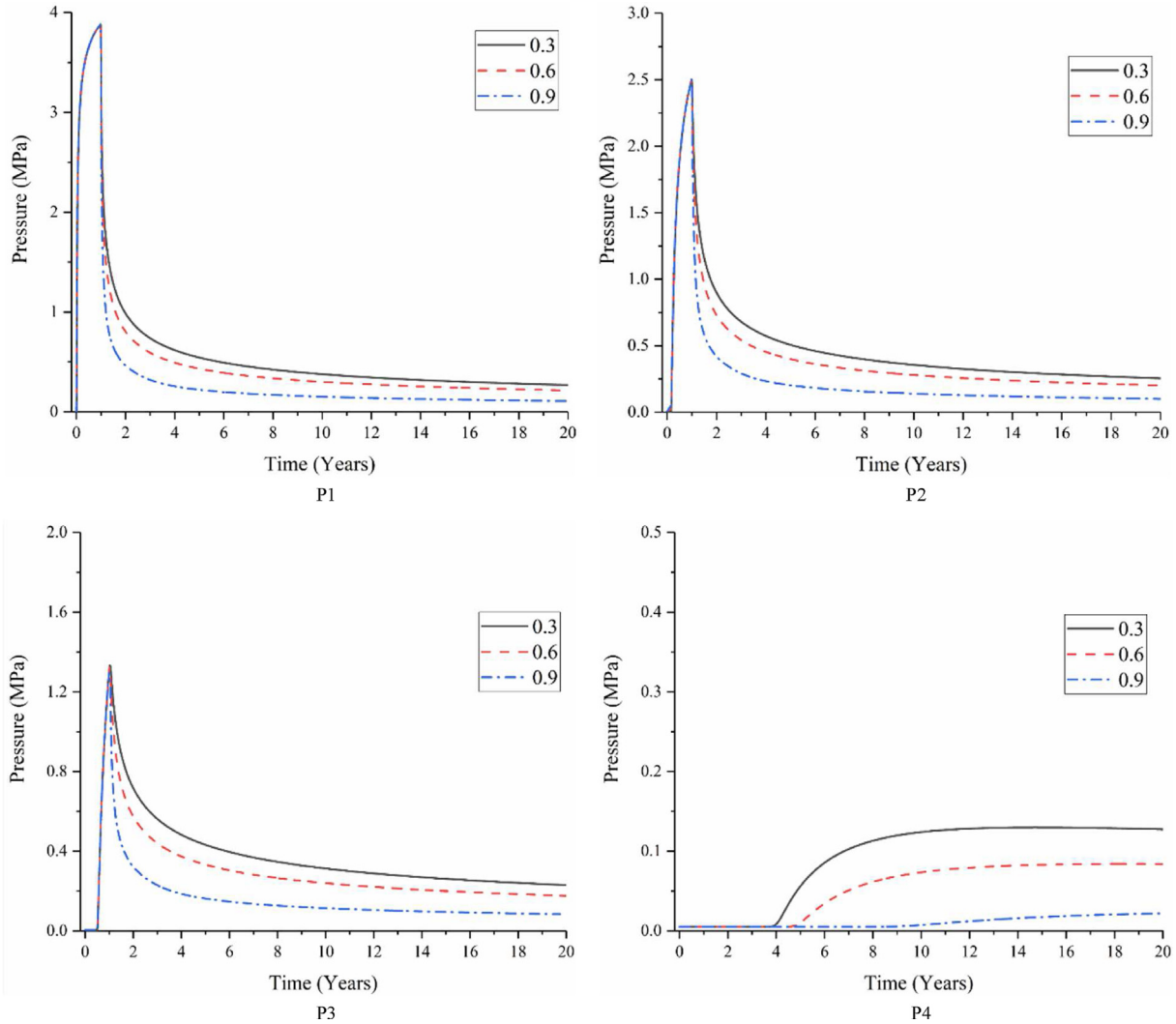

Fig. 13. Comparison of pressure evolutions at monitoring points P1–P4 between different degrees of hysteresis.

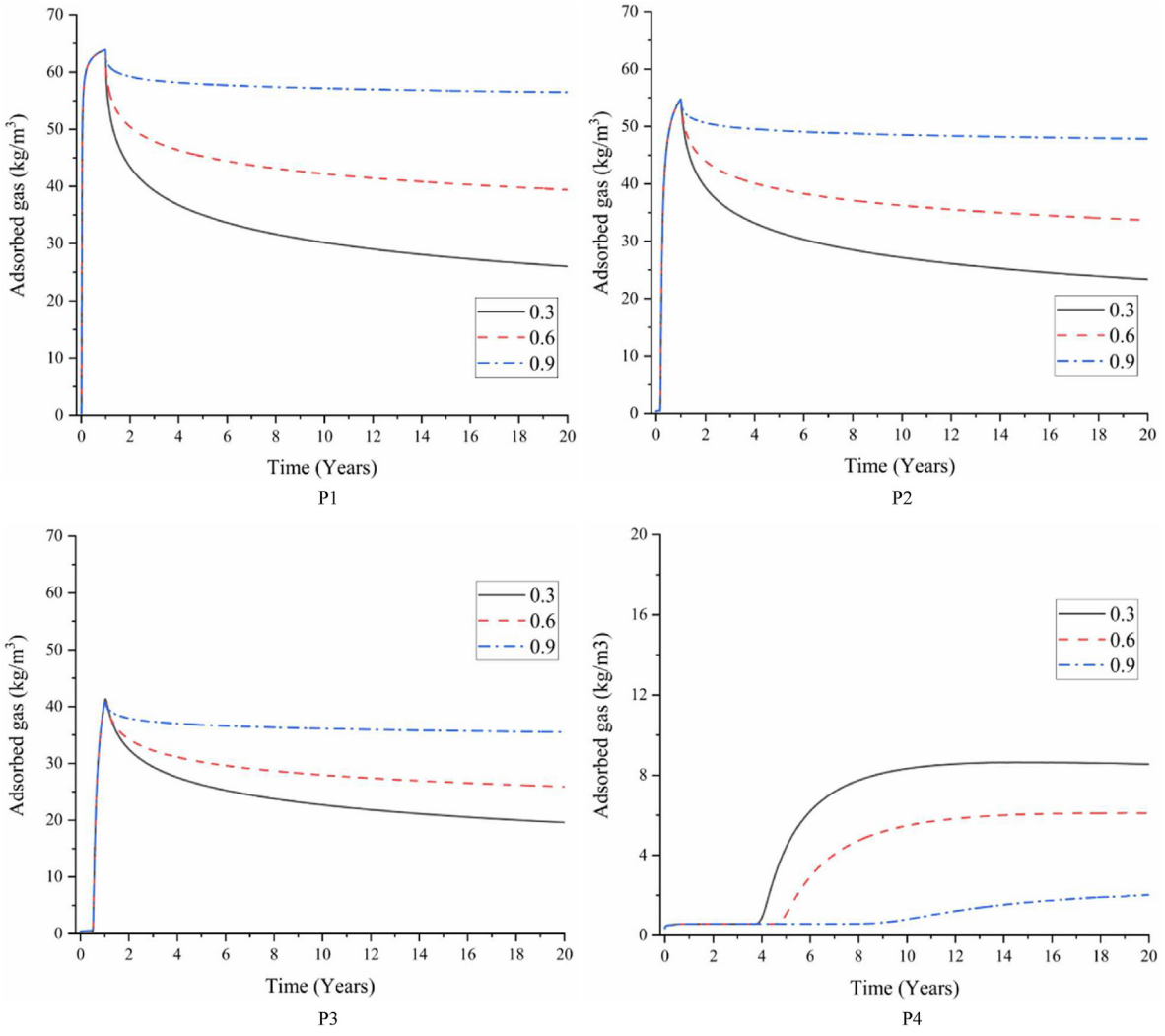

Fig. 14. Comparison of adsorbed gas concentration evolutions at monitoring points P1–P4 between different degrees of hysteresis.

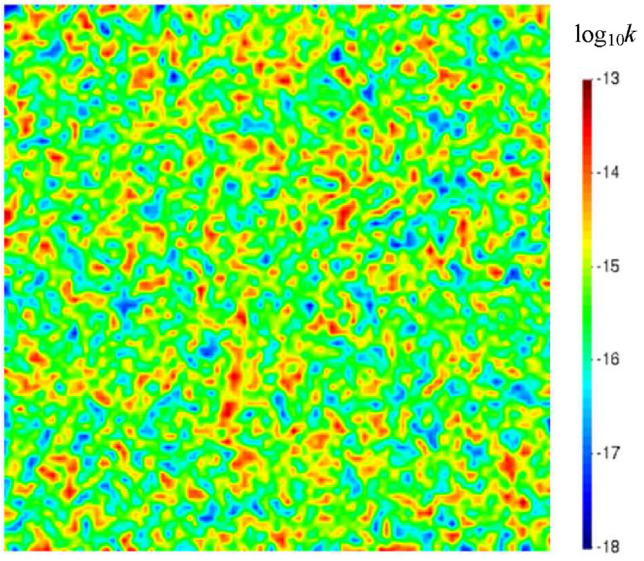

Fig. 15. Permeability field.

tion well and enough reservoir area should be considered for long term safety of CO_2 storage since the injected CO_2 will continue to spread after injection stops. The effect of reservoir heterogeneity should not be ignored when designing the geological CO_2 storage, advanced geostochastic methods like Kriging distribution can be used for accurate representation of reservoir heterogeneity.

6. Conclusions

To unlock the sustained effectiveness of CO_2 storage into coal reservoirs, this paper firstly develops a new adsorption-desorption isotherm of gases in coals with considering desorption hysteresis. Particularly, a hysteresis index, which is applied to quantify the degree of hysteresis, is derived based on thermodynamics. And then the developed adsorption-desorption model is incorporated into a numerical model of coupled gas flow and deformation behaviour. The ability of the proposed model is demonstrated through validation tests against laboratory experiments. The temporal-spatial evolutions of pressure and adsorbed CO_2 during injection and post-injection periods of operations are investigated. The major observations include:

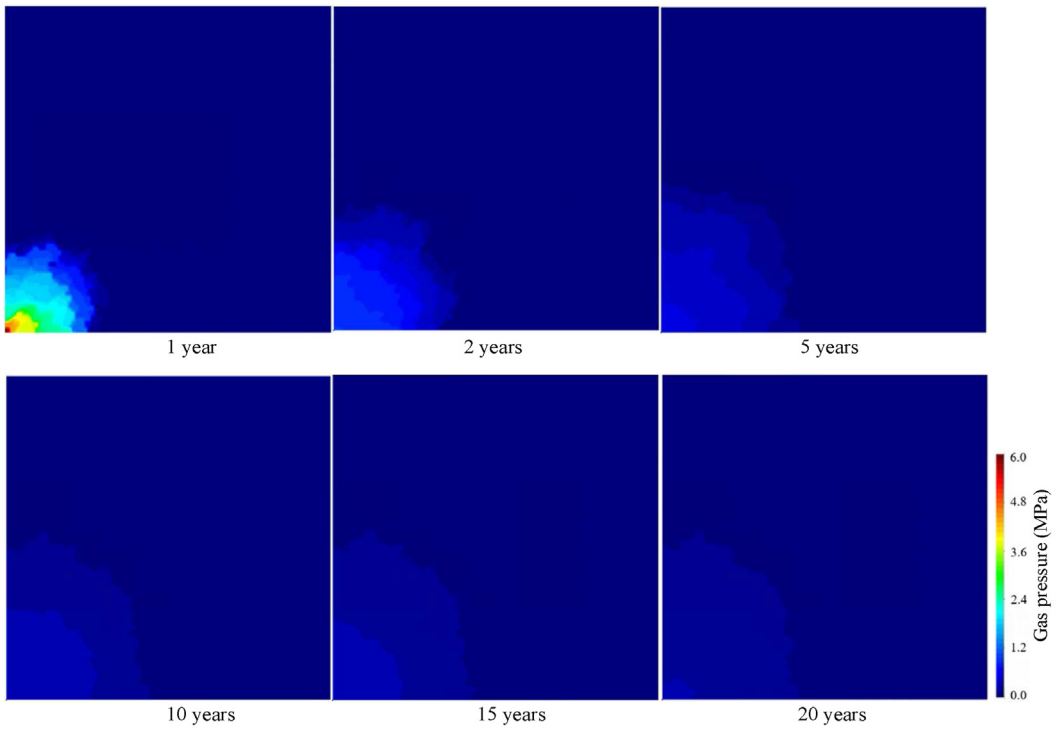

Fig. 16. Pressure distribution in the heterogeneous coal seam after 1 year, 2 years, 5 years, 10 years, 15 years and 20 years.

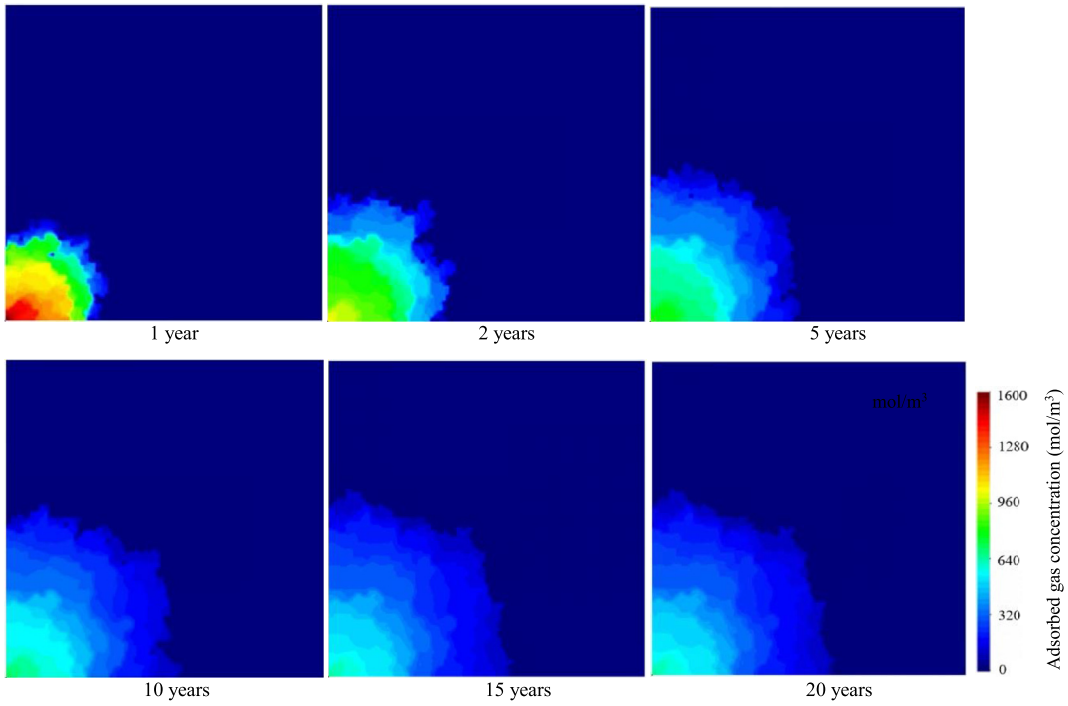

Fig. 17. Adsorbed gas concentration distribution in the heterogeneous coal seam after 1 year, 2 years, 5 years, 10 years, 15 years and 20 years.

(1) Adsorption induced pore deformation is the mechanism behind desorption hysteresis. There is more pores with smaller size after adsorption, this leads to an increase in adsorption sites with higher binding energy, the release of adsorbed gas requires greater activation energy generated by a larger decrease in gas pressure.

(2) Injected gas continues to propagate after injection stop. Gas pressure near the injection well experiences a significant drop after injection stop, which causes a drop in the pressure difference in the domain. In comparison, the differences in adsorbed CO_2 concentration in the domain are obvious due to desorption hysteresis.

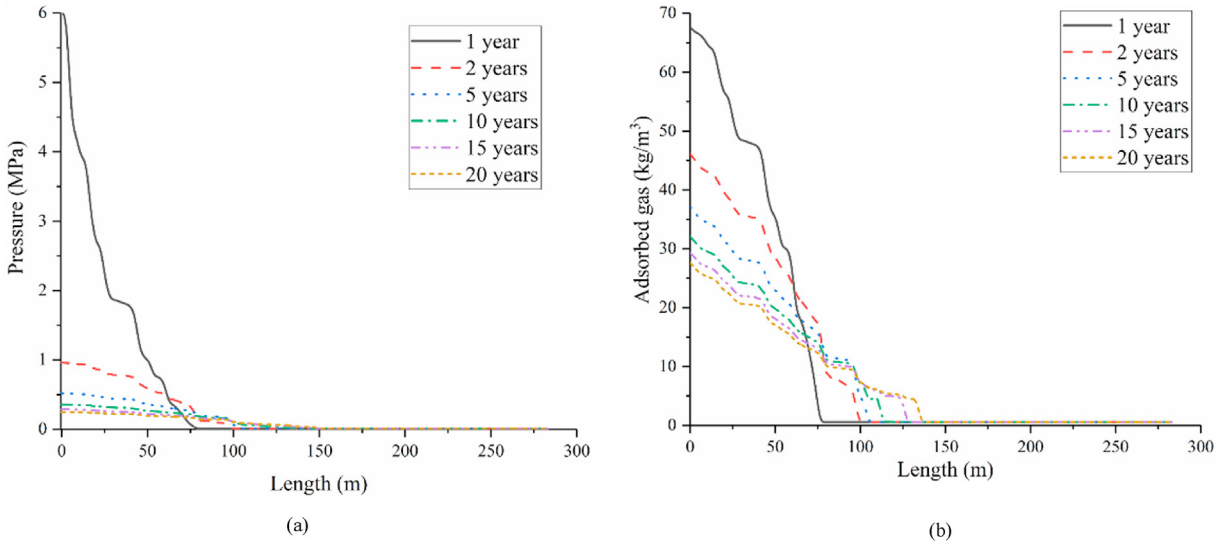

Fig. 18. Pressure and adsorbed gas concentration distribution along the diagonal of heterogeneous domain at different times: (a) Pressure and (b) adsorbed gas concentration.

(3) The continuous propagation of injected CO_2 within coal seams and drops of pressure and adsorbed gas as time increases are associated with the degree of desorption hysteresis and heterogeneity of coal seams. The stronger degree of hysteresis is, the more significant drop in pressure near injection well, but the drop of adsorbed gas concentration is less. The spread of gas in heterogeneous coal seams is obviously slower compared to the homogeneous case, thus, the heterogeneity effect on gas flow should be considered when designing CO_2 geological sequestration.

Declaration of competing interest

The authors declare that they have no known competing financial interests or personal relationships that could have appeared to influence the work reported in this paper.

Acknowledgments

The research was conducted as part of the “Establishing a Research Observatory to Unlock European Coal Seams for CO_2 Storage (ROCCS)” project (Grant No. 899336). The work of the second author is also sponsored by Shanghai Pujiang Program (Grant No. 23PJ1412600). The financial support is also gratefully acknowledged.

Appendix A. Supplementary data

Supplementary data to this article can be found online at https://doi.org/10.1016/j.jrmge.2023.11.004.

References

Abbass, K., Qasim, M.Z., Song, H., Murshed, M., Mahmood, H., Younis, I., 2022. A review of the global climate change impacts, adaptation, and sustainable mitigation measures. Environ. Sci. Pollut. Res. 29, 42539–42559.

Al-Yasiri, Q., Géczi, G., 2021. Global warming potential: causes and consequences. Acad. Lett. https://doi.org/10.20935/AL3202.

Ali, M., Jha, N.K., Pal, N., Keshavarz, A., Hoteit, H., Sarmadivaleh, M., 2022. Recent advances in carbon dioxide geological storage, experimental procedures, influencing parameters, and future outlook. Earth Sci. Rev. 225, 103895.

Asif, M., Wang, L., Wang, R., Wang, H., Hazlett, R.D., 2022. Mechanisms in CO_2-enhanced coalbed methane recovery process. Adv. Geo-Energy Res. 6 (6), 531–534.

Bell, G.J., Rakop, K.C., 1986. Hysteresis of methane/coal sorption isotherms. In: Proceedings of the SPE Annual Technical Conference and Exhibition.

Burhan, M., Shahzad, M.W., Ng, K.C., 2019. A universal theoretical framework in material characterization for tailored porous surface design. Sci. Rep. 9, 1–7.

Busch, A., Gensterblum, Y., 2011. CBM and CO_2-ECBM related sorption processes in coal: a review. Int. J. Coal Geol. 87, 49–71.

Chattaraj, S., Mohanty, D., Kumar, T., Halder, G., 2016. Thermodynamics, kinetics and modeling of sorption behaviour of coalbed methane–A review. J. Unconv. Oil Gas Resour. 16, 14–33.

Chen, M., Hosking, L.J., Sandford, R.J., Thomas, H.R., 2019. Dual porosity modelling of the coupled mechanical response of coal to gas flow and adsorption. Int. J. Coal Geol. 205, 115–125.

Chen, M., Masum, S., Sadasivam, S., Thomas, H., 2022a. Modelling anisotropic adsorption-induced coal swelling and stress-dependent anisotropic permeability. Int. J. Rock Mech. Min. Sci. 153, 105107.

Chen, M., Masum, S., Thomas, H., 2022b. 3D hybrid coupled dual continuum and discrete fracture model for simulation of CO_2 injection into stimulated coal reservoirs with parallel implementation. Int. J. Coal Geol., 104103

Chen, M., Masum, S.A., Sadasivam, S., Thomas, H.R., Mitchell, A.C., 2023. Modeling gas adsorption–desorption hysteresis in energetically heterogeneous coal and shale. Energy Fuel. 37 (3), 2149–2163.

Cheng, Y., Zhang, X., Lu, Z., Pan, Z.J., Zeng, M., Du, X., Xiao, S., 2021. The effect of subcritical and supercritical CO_2 on the pore structure of bituminous coals. J. Nat. Gas Sci. Eng. 94, 104132.

Cui, X., Bustin, R.M., Chikatamarla, L., 2007. Adsorption-induced coal swelling and stress: implications for methane production and acid gas sequestration into coal seams. J. Geophys. Res. 112.

Cui, L.Y., Masum, S.A., Ye, W.M., Thomas, H.R., 2022. Investigation on gas migration behaviours in saturated compacted bentonite under rigid boundary conditions. Acta Geotech 1–15.

Do, D.D., 1998. Adsorption Analysis: Equilibria and Kinetics. Imperial College Press, London, UK.

Do, D., Wang, K., 1998. A new model for the description of adsorption kinetics in heterogeneous activated carbon. Carbon 36, 1539–1554.

Dobruskin, V.K., 1998. Physical adsorption in micropores: a condensation approximation approach. Langmuir 14, 3847–3857.

Dutta, P., Bhowmik, S., Das, S., 2011. Methane and carbon dioxide sorption on a set of coals from India. Int. J. Coal Geol. 85, 289–299.

Fujioka, M., Yamaguchi, S., Nako, M., 2010. CO_2-ECBM field tests in the ishikari coal basin of Japan. Int. J. Coal Geol. 82, 287–298.

Geng, W., Huang, G., Guo, S., Jiang, C., Dong, Z., Wang, W., 2022. Influence of long-term CH_4 and CO_2 treatment on the pore structure and mechanical strength characteristics of Baijiao coal. Energy 242, 122986.

Godec, M., Koperna, G., Gale, J., 2014. CO_2-ECBM: a review of its status and global potential. Energy Proc. 63, 5858–5869.

Gu, F., Chalaturnyk, R., 2006. Numerical simulation of stress and strain due to gas sorption/desorption and their effects on in situ permeability of coalbeds. J. Can. Pet. Technol. 45.

Hosking, L.J., Thomas, H.R., Sedighi, M., 2017. A dual porosity model of high-pressure gas flow for geoenergy applications. Can. Geotech. J. 55, 839–851.

Hosking, L.J., Chen, M., Thomas, H.R., 2020. Numerical analysis of dual porosity coupled thermo-hydro-mechanical behaviour during CO_2 sequestration in coal. Int. J. Rock Mech. Min. Sci. 135, 104473.

Kuang, N.J., Zhou, J.P., Xian, X.F., Zhang, C.P., Yang, K., Dong, Z.Q., 2023. Geomechanical risk and mechanism analysis of CO2 sequestration in unconventional coal seams and shale gas reservoirs. Rock Mechanics Bulletin 2, 100079.
Larsen, J.W., 2004. The effects of dissolved CO_2 on coal structure and properties. Int. J. Coal Geol. 57, 63–70.
Li, J., Wu, K., Chen, Z., Wang, W., Yang, B., Wang, K., Luo, J., Yu, R., 2019. Effects of energetic heterogeneity on gas adsorption and gas storage in geologic shale systems. Appl. Energy 251, 113368.
Liu, Q., Cheng, Y., Zhou, H., Guo, P., An, F., Chen, H., 2015. A mathematical model of coupled gas flow and coal deformation with gas diffusion and Klinkenberg effects. Rock Mech. Rock Eng. 48, 1163–1180.
Masson-Delmotte, V., Zhai, P., Pörtner, H.-O., Roberts, D., Skea, J., Shukla, P.R., 2022. Global Warming of 1.5 °C: IPCC Special Report on Impacts of Global Warming of 1.5 °C above Pre-industrial Levels in Context of Strengthening Response to Climate Change, Sustainable Development, and Efforts to Eradicate Poverty. Cambridge University Press, UK.
Mavor, M.J., Gunter, W.D., Robinson, J.R., Law, D.H., Gale, J., 2002. Testing for CO_2 sequestration and enhanced methane production from coal. In: Proceedings of the SPE Gas Technology Symposium. Society of Petroleum Engineers.
Meng, Y., Li, Z., 2017. Triaxial experiments on adsorption deformation and permeability of different sorbing gases in anthracite coal. J. Nat. Gas Sci. Eng. 46, 59–70.
Mito, S., Xue, Z., 2011. Post-Injection monitoring of stored CO_2 at the Nagaoka pilot site: 5 years time-lapse well logging results. Energy Proc. 4, 3284–3289.
NASA, 2017. NASA, NOAA Data Show 2016 Warmest Year on Record Globally. https://www.nasa.gov/news-release/nasa-noaa-data-show-2016-warmest-year-on-record-globally/.
Ng, K.C., Burhan, M., Shahzad, M.W., Ismail, A.B., 2017. A universal isotherm model to capture adsorption uptake and energy distribution of porous heterogeneous surface. Sci. Rep. 7, 1–11.
Özgen Karacan, C., Okandan, E., 1999. Heterogeneity effects on the storage and production of gas from coal seams. In: Proceedings of the SPE Annual Technical Conference and Exhibition. https://doi.org/10.2118/56551-MS.
Pan, Z., Connell, L.D., Camilleri, M., 2010. Laboratory characterisation of coal reservoir permeability for primary and enhanced coalbed methane recovery. Int. J. Coal Geol. 82, 252–261.
Pan, Z., Connell, L.D., 2012. Modelling permeability for coal reservoirs: a review of analytical models and testing data. Int. J. Coal Geol. 92, 1–44.
Panczyk, T., Rudzinski, W., 2002. Kinetics of multisite-occupancy adsorption on heterogeneous solid surfaces: a statistical rate theory approach. J. Phys. Chem. B 106, 7846–7851.
Pao, W.K., Lewis, R.W., 2002. Three-dimensional finite element simulation of three-phase flow in a deforming fissured reservoir. Comput. Methods Appl. Mech. Eng. 191, 2631–2659.
Peng, D.-Y., Robinson, D.B., 1976. A new two-constant equation of state. Ind. Eng. Chem. Fundam. 15, 59–64.
Reeves, S., Taillefert, A., Pekot, L., Clarkson, C., 2003. The Allison unit CO_2–ECBM pilot: a reservoir modeling study. Advanced Resources International. https://doi.org/10.2172/825083. Technical Report FC26-00NT40924.
Reisabadi, M.Z., Sayyafzadeh, M., Haghighi, M., 2022. Stress and permeability modelling in depleted coal seams during CO_2 storage. Fuel 325, 124958.
Ritchie, H., Roser, M., Rosado, P., 2020. CO_2 and Greenhouse Gas Emissions. Our World in Data.
Sander, M., Lu, Y., Pignatello, J.J., 2005. A thermodynamically based method to quantify true sorption hysteresis. J. Environ. Qual. 34, 1063–1072.
Seidle, J.R., Huitt, L., 1995. Experimental measurement of coal matrix shrinkage due to gas desorption and implications for cleat permeability increases. In: Proceedings of the International Meeting on Petroleum Engineering. Society of Petroleum Engineers.
Strapoc, D., 2007. Coalbed Gas Origin and Distribution in the Southeastern Illinois Basin. Indiana University, USA.
Tan, Y., Pan, Z., Liu, J., Zhou, F., Connell, L.D., Sun, W., Haque, A., 2018. Experimental study of impact of anisotropy and heterogeneity on gas flow in coal. Part II: permeability. Fuel 230, 397–409.
Thomas, H., He, Y., 1997. A coupled heat–moisture transfer theory for deformable unsaturated soil and its algorithmic implementation. Int. J. Numer. Methods Eng. 40, 3421–3441.
Tomić, L., Karović-Maričić, V., Danilović, D., Crnogorac, M., 2018. Criteria for CO_2 storage in geological formations. Podzemni Radovi 2018 (32), 61–74.
van Bergen, F., Pagnier, H., Krzystolik, P., 2006. Field experiment of enhanced coalbed methane-CO_2 in the upper Silesian basin of Poland. Environ. Geosci. 13, 201–224.
Wang, K., Wang, G., Ren, T., Cheng, Y., 2014. Methane and CO_2 sorption hysteresis on coal: a critical review. Int. J. Coal Geol. 132, 60–80.
Wang, D., Lv, R., Wei, J., Zhang, P., Yu, C., Yao, B., 2018a. An experimental study of the anisotropic permeability rule of coal containing gas. J. Nat. Gas Sci. Eng. 53, 67–73.
Wang, Z., Cheng, Y., Zhang, K., Hao, C., Wang, L., Li, W., Hu, B., 2018b. Characteristics of microscopic pore structure and fractal dimension of bituminous coal by cyclic gas adsorption/desorption: an experimental study. Fuel 232, 495–505.
Ward, C.R., Suárez-Ruiz, I., 2008. Introduction to applied coal petrology. Appl. Coal Pet. 1–18.
Wei, B., Wang, B., Li, X., Aishan, M., Ju, Y., 2023. CO_2 storage in depleted oil and gas reservoirs: a review. Adv. Geo-Energy Res. 9, 76–93.
Weishauptová, Z., Medek, J., Kovář, L., 2004. Bond forms of methane in porous system of coal II. Fuel 83, 1759–1764.
Wierzbicki, M., Konecny, P., Kozusnikova, A., 2014. Permeability changes of coal cores and briquettes under tri-axial stress conditions. Arch. Min. Sci. 59 (4), 1131–1140.
Wong, S., Law, D., Deng, X., Robinson, J., Kadatz, B., Gunter, W.D., Jianping, Y., Sanli, F., Zhiqiang, F., 2007. Enhanced coalbed methane and CO_2 storage in anthracitic coals—micro-pilot test at South Qinshui, Shanxi, China. Int. J. Greenh. Gas Control 1, 215–222.
Yang, Y., Clarkson, C.R., Hamdi, H., Ghanizadeh, A., Blinderman, M.S., Evans, C., 2023. Field pilot testing and reservoir simulation to evaluate processes controlling CO_2 injection and associated in-situ fluid migration in deep coal. Int. J. Coal Geol. 275, 104317.
Yao, H., Chen, Y., Liang, W., Li, Z., Song, X., 2023. Experimental study on the permeability evolution of coal with CO_2 phase transition. Energy 266, 126531.
Yoro, K.O., Daramola, M.O., 2020. CO_2 Emission Sources, Greenhouse Gases, and the Global Warming Effect, Advances in Carbon Capture. Elsevier, pp. 3–28.
Zhang, X.G., Ranjith, P.G., Perera, M.S.A., Ranathunga, A.S., Haque, A., 2016. Gas Transportation and enhanced coalbed methane recovery processes in deep coal seams: A review. Energy Fuel. 30, 8832–8849.
Zhang, X., Wu, C., Wang, Z., 2019. Experimental study of the effective stress coefficient for coal permeability with different water saturations. J. Pet. Sci. Eng. 182, 106282.
Zhou, Y., Zhang, R., Wang, J., Huang, J., Li, X., Wu, J., 2020. Desorption hysteresis of CO_2 and CH4 in different coals with cyclic desorption experiments. J. CO_2 Util. 40, 101200.

Dr. Hywel Thomas is Professor of Civil Engineering at Cardiff University, UK; the founder Director of the Geo-environmental Research Centre (GRC) at the University. His research interests lie in the area of "Coupled processes in the Ground". Current interests are focused on the geo-energy field, with major projects on ground source heat, underground coal gasification, exploitation of unconventional gas and carbon sequestration in coal seams. His academic achievements have been recognised by election as a Fellow of the Royal Society (FRS) in 2003. He is also a Fellow of the Royal Academy of Engineering (FREng) in 2012. He has also been elected a Member of Academia Europaea, the Academy of Europe (MAE) and was recently elected a Foreign Member of the Chinese Academy of Sciences. In 2017 he received a CBE in the New Year's Honours List for "Services to Academic Research and Higher Education".